Appl. Phys. B 65, 693–700 (1997)

Applied Physics B Lasers and Optics

Quantum transport of ultracold atoms in an accelerating optical potential

K.W. Madison, C.F. Bharucha*, P.R. Morrow, S.R. Wilkinson***, Q. Niu, B. Sundaram****, M.G. Raizen*****

Department of Physics, The University of Texas at Austin, Austin, Texas 78712-1081, USA

Received: 8 July 1997

Abstract. We review our recent experiments on the motion of ultracold sodium atoms in an accelerating one-dimensional standing wave of light. Atoms are trapped in a far-detuned standing wave that is accelerated for a controlled duration. A small oscillatory component is added to the acceleration, and the fraction of trapped atoms is measured as a function of the oscillation frequency. Resonances are observed where the number of trapped atoms drops dramatically. The separation between resonances is found to be proportional to the acceleration, and they are identified as a Wannier–Stark ladder. At higher values of the acceleration, we observe an exponential decay in the number of atoms that remain trapped as a function of the interaction time. This loss is due to quantum tunneling, and we compare the decay rates with Landau–Zener theory. We also observe oscillations in the tunneling rate as a function of the acceleration; these are due to quantum interference effects.

PACS: 03.75.-b; 32.80.Pj

Quantum transport of particles in spatially tailored potentials has been a topic of active research in recent years, motivated by fundamental interest and by the prospect of controlling electron motion in microfabricated devices. In the regime of quantum transport, motion is dominated by tunneling and interference over macroscopic regions of phase space, and there are many basic questions that remain to be studied. The simplest case of a periodic potential was first studied theoretically in the 1930s by Bloch and Zener as a model of electron conduction in a crystalline lattice [1, 2]. A periodic potential in one dimension leads to a quantized energy structure as shown in Fig. 1 for the case of a cosine potential [3]. The levels are broadened into bands due to resonant tunneling between adjacent wells. As the well depth is increased, tunneling in the low-lying bands is suppressed, and particle motion is dominated by single-well dynamics. Near the bottom of the well, the harmonic approximation is valid, further simplifying the analysis. This same band structure can also be displayed in the reciprocal lattice, as shown in Fig. 2. This plot is a dispersion relation between the energy E and the quasi-momentum $\hbar k$ (also referred to in textbooks as the crystal momentum). As a familiar point of reference, free particle motion would be represented in this picture as a parabola, due to the quadratic dependence of energy on quasi-momentum. The parabola is distorted when the periodic potential is turned on, opening band gaps. Note that the quasi-momentum is restricted here to the first Brillouin zone [3]. The natural basis set for this problem is composed of Bloch states that are spatially delocalized. An initial atomic wave packet that is spatially localized will then spread via resonant "Bloch" tunneling.

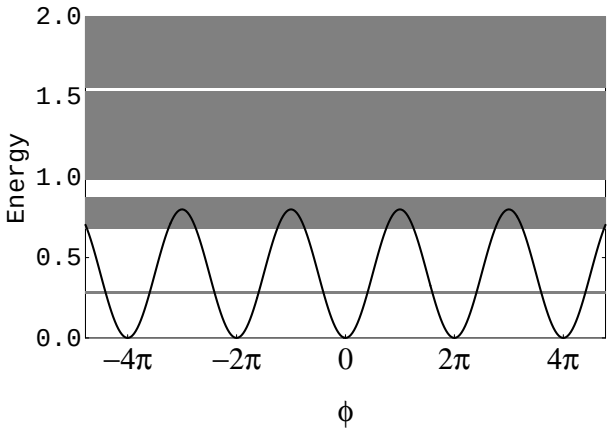

Fig. 1. The band structure of an optical lattice, with $V_0/h = 68$ kHz. The curved line is the periodic potential plotted as a function of position, ϕ. The allowed energy bands are the shaded regions, while the energy gaps are blank. The unit of energy is 200 kHz and $\phi = 2k_{\mathrm{L}}x$

* Present address: Conley, Rose and Tayon, P.C., 816 Congress Ave., Austin, TX 78701, USA

** Present address: Intel Corp., 5200 NE Elam Young Pkwy, Hillsboro, OR 97124, USA

*** Present address: Hughes Aircraft Co., 2000 E. El Segundo Blvd., El Segundo CA 90245, USA

**** Present address: Department of Mathematics, CSI-CUNY, Staten Island, NY 10314, USA

***** Correspondence to: raizen@physics.utexas.edu

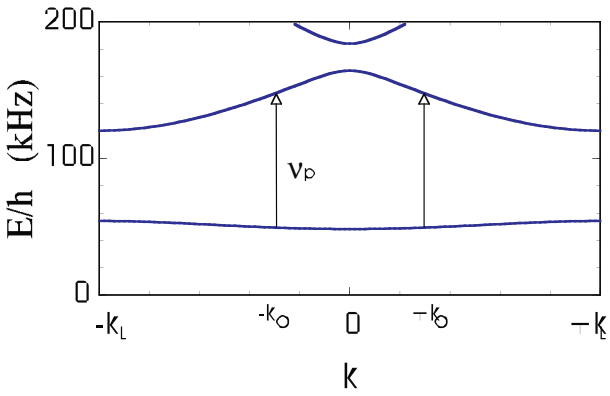

Fig. 2. The band structure of an optical lattice, with $V_0/h = 68$ kHz. This is shown for the reciprocal lattice in the reduced zone scheme, limited to the first Brillouin zone, $[-k_L, +k_L]$

The situation becomes much more complicated when the translational symmetry is broken. This occurs, for example, in a tilted periodic potential which is used as a model for electron conduction in a DC electric field. More generally, the tilt is caused by a force F along the direction of the potential. In the band picture, the quasi-momentum ($\hbar k$) changes in time and the particles move periodically across the first Brillouin zone, a phenomenon known as Bloch oscillations. The Bloch period, T_B, is given by $T_B = h/Fd$, where d is the lattice period. The quantized energy structure is also changed when a tilt is imposed; the Bloch bands break up into a set of equally spaced energy levels, referred to as a Wannier–Stark ladder, with a level spacing given by h/T_B [4]. The Wannier–Stark ladder marked such a dramatic departure from the Bloch bands that this prediction was very controversial [5]. In addition to "Bloch" tunneling, interband tunneling, known as Landau–Zener tunneling [2, 6], can occur for tilts that are much smaller than the classical limit (where there are no local minima in the potential).

Bloch oscillations and Wannier–Stark ladders have not been observed in a crystalline solid because scattering by impurities, phonons and other particles effectively destroys the required quantum coherence. Another problem is that the natural lattice spacing is very small (several angstroms), requiring very large electric fields to obtain a substantial tilt of the potential. The situation becomes much more favorable in superlattices that are fabricated by epitaxial growth of GaAs and GaAlAs. The lattice constant of these structures can be hundreds of angstroms, yielding a much shorter Bloch period under the same electric field. In the late 1980s, Wannier–Stark ladders were seen in optical absorption and photocurrent measurements of superlattices. Evidence for Bloch oscillations was seen in the time domain using the technique of four-wave mixing with picosecond lasers (for a recent review, see [7]).

These results represent an important breakthrough in the study of quantum transport of electrons: however, many challenges remain. Dissipation and elastic scattering by impurities are still a central problem limiting the coherent evolution required for quantum transport. This is evident in the broad line shapes that smear out spectral and temporal detail. The control of initial conditions is difficult in condensed matter experiments, and direct measurement of electron motion is not possible. This provides motivation for the identification of a new testing ground for these striking quantum phenomena that can complement the superlattice experiments.

1 Wannier–Stark ladders

The development of techniques for laser cooling and trapping of neutral atoms has opened up a new experimental arena for the study of quantum transport [8]. These systems use atoms instead of electrons and a periodic light field instead of the periodic crystalline potential. The advantages of this approach are precise initial state preparation and final detection, negligible dissipation or defects, and the possibility of time-resolved measurements of quantum transport. We review here our recent observations of Wannier–Stark ladders and Landau–Zener tunneling with ultracold sodium atoms in an accelerating optical lattice [9–11]. In parallel with this work, a group at ENS in Paris has observed Bloch oscillations in time domain as well as Landau–Zener tunneling [12, 13].

Consider atomic motion in an accelerating potential of the form $V_0 \cos[2k_L x - k_L a t^2]$, where a is the acceleration [14]. In the reference frame of the standing wave, this potential becomes

$$V_0 \cos(2k_L x') + Max' \,, \tag{1}$$

where M is the mass of the atom and x' is the position in the co-moving frame. Atoms that are trapped and accelerated will experience this tilted potential. This equation is analogous to the condensed-matter problem of an electron in a periodic lattice, with an applied DC electric field, where the term Ma is replaced by eE. In our case the periodic potential can be created by a standing wave of light formed by two counterpropagating beams that are tuned far from an atomic resonance. In this regime, an atom experiences a potential of the ground state given by $V_0 \cos(2k_L x)$, where V_0 is known as the optical dipole potential [15], and spontaneous scattering can be neglected.

The acceleration of the standing wave is accomplished by chirping the frequency difference of the two counterpropagating beams. This method is commonly used with resonant light in atomic-fountain clocks to launch atoms upward [16]. To describe this method in more detail, suppose first that, instead of forming the standing wave with two counterpropagating beams having equal frequencies ν_L, the beam coming from the left is up-shifted by a small amount $\delta\nu$, while the beam coming from the right is down-shifted by the same amount. In the reference frame moving to the right at a velocity $v = \lambda\delta\nu$, the two beams are Doppler shifted to the same frequency and the periodic potential is stationary in this frame. Now suppose that $\delta\nu$ is increased linearly with time between zero and a maximum value $\delta\nu_{\max}$ in a given time t_a. This produces in the laboratory frame a potential that is uniformly accelerated with an acceleration proportional to $\delta\dot{\nu}$ during t_a. In contrast to resonant atom–light interactions, the large detuning from resonance in the present work leads to a coherent atom–field interaction that is dissipation-free. In the co-moving frame, the atoms experience an inertial force proportional to the acceleration, in addition to the force resulting from the periodic potential.

In order to observe the Wannier–Stark ladder, we add a phase modulation at ν_p to the accelerating optical potential. The potential then becomes $V_0 \cos[2k_L x - k_L a t^2 +$

$\lambda\cos(2\pi\nu_p t)]$, where λ is the modulation amplitude. Transforming to the co-moving frame, x', the potential becomes

$$V_0\cos(2k_L x') + Max' + \frac{(2\pi\nu_p)^2 M\lambda}{2k_L}x'\cos(2\pi\nu_p t)\,, \qquad (2)$$

The third term in this expression plays the role of an AC field that can drive resonant transitions between the first two bands, as indicated by the arrows in Fig. 3. For appropriate values of the acceleration, the tunneling rate from the lowest band is negligible, while the tunneling rate from higher bands is large [9] due to the smaller band gaps. Therefore only the atoms in the lowest band are accelerated, while atoms in the higher bands are left behind. By applying a weak phase modulation and measuring the number of atoms that are accelerated, the probability of excitation can be studied. A theoretical analysis of this problem shows that the transition probability as a function of modulation frequency displays several equally spaced resonances, which are identified as an atomic Wannier–Stark ladder [9].

The experimental study of this system relies on cooling and trapping of sodium atoms to prepare the initial conditions. A magneto-optic trap (MOT) is used to trap and cool the sodium atoms [15]. A single-mode dye laser locked near the sodium D_2 transition at 589 nm is used for the trapping and cooling, and the details are described in [10]. A cloud of approximately 10^5 atoms forms a spatial Gaussian distribution with $\sigma_x = 0.12$ mm. This sample is sufficiently dilute that atom–atom interactions are negligible over the time scale of the experiment. The Gaussian momentum distribution has a width of $\sigma_p = 5\hbar k_L$, centered at $p = 0$. After the cooling and trapping stage, the MOT beams and magnetic field gradient are turned off.

The accelerating standing wave is provided by a second single-mode dye laser tuned far (up to 20 GHz) from atomic resonance. The optical setup is shown in Fig. 4. The beams are linearly polarized (so that atoms in different magnetic sublevels experience the same dipole potential), spatially filtered and aligned on the trapped atoms in a counterpropagating configuration, with a beam waist of 2.4 mm in the center of the trap. The beams are turned on simultaneously (in less than 150 ns) and a subset of atoms is trapped within the first Brillouin zone and accelerated. This method selects a two-photon recoil window in momentum from the center of the initial thermal distribution. Atoms with a momentum that is outside this window will be projected into higher bands, but will not track the accelerations imposed.

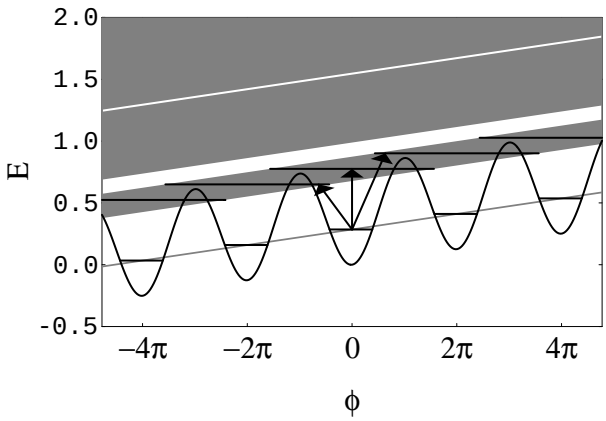

Fig. 3. Tilted bands and Wannier–Stark ladders for $V_0/h = 80$ kHz and 1500 m/s^2. Arrows indicate resonant excitations by an AC modulation of the acceleration. The unit of energy is 200 kHz and $\phi = 2k_L x$

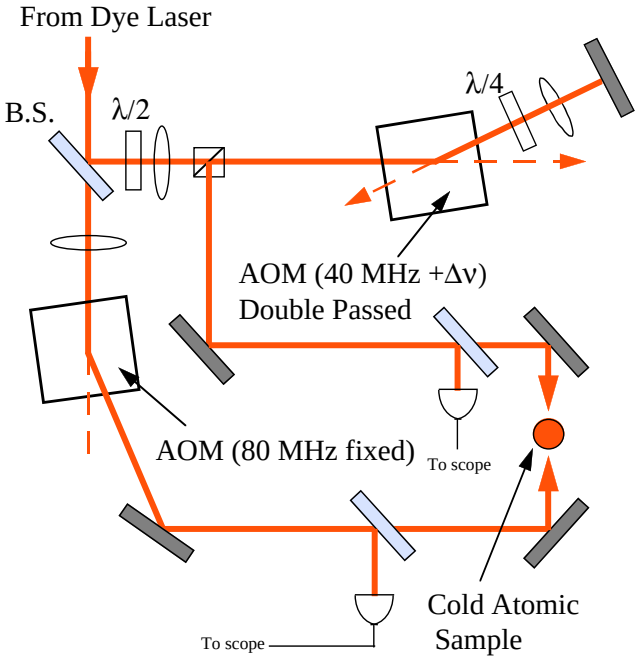

Fig. 4. The experimental setup for the accelerating standing wave. The output of a dye laser is divided using a beam splitter (B.S.). One arm is aligned through an 80 MHz acousto-optical modulator (AOM). The other arm is aligned in a double pass configuration through a 40 MHz AOM. The two beams are aligned on the atoms in a counterpropagating configuration. When the frequency of the double-pass AOM is set to 40 MHz, the standing wave pattern is stationary in the laboratory frame. The acceleration is imposed by ramping the drive frequency of that AOM linearly in time. For the Wannier–Stark experiments, the double-pass arm also had an electro-optical phase modulator (not shown in the figure)

As described above, the standing wave is accelerated by varying the frequency difference of its two beams linearly in time. As an example, a linear ramp of 4 MHz in 800 μs (in one beam) creates an accelerating potential of 1500 m/s^2. In the experiments described here, accelerations of up to 1800 m/s^2 were used, with interaction times of up to 1 ms. For these parameters, the Landau–Zener tunneling rate from the lowest band is negligible, as described earlier. The final velocity of the standing wave was chosen to be 1.2 m/s (a momentum of $40\hbar k_L$), which is sufficient to distinguish the trapped atoms from the rest of the distribution.

After interacting with the accelerating standing wave the atoms drift in the dark for 3 ms, and then the trapping beams are turned back on without the magnetic field gradient, forming optical molasses [15]. The motion of the atoms in the molasses is effectively frozen for short times, during which the fluorescence is recorded on a CCD camera [17]. The resulting 2-D images are integrated to give the 1-D distribution along the standing-wave axis. The final distributions are characterized by two peaks: the larger one centered around $x = 0$ corresponds to atoms that are not trapped by the standing wave. The smaller peak is from the atoms that were trapped, and is centered around $x = 3.5$ mm. Examples of these distributions are shown in Fig. 5. The distribution in Fig. 5a was made with the phase modulation off and was

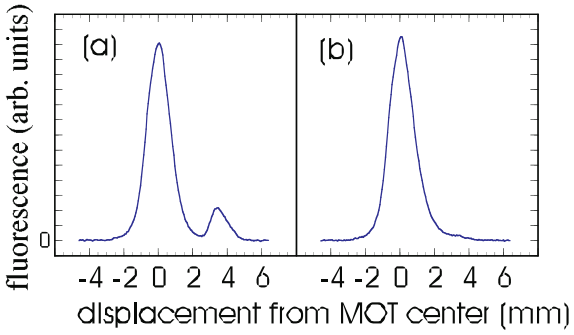

Fig. 5a,b. The distribution of atoms after exposure to an accelerating standing wave. The displacement is the distance from the atoms' initial location in the magneto-optic trap. The fluorescence is proportional to the number of atoms at a given displacement. In **a** a fraction of the atoms was trapped by the standing wave and accelerated for 650 μs to a final velocity of 1.2 m/s. The atoms then drifted ballistically for 3 ms, allowing them to separate spatially from the main distribution. Here $V_0/h = 68$ kHz. In **b** the fraction of trapped atoms was dramatically reduced by adding a modulation $\lambda = 0.13$ to the standing wave at a frequency of $\nu_p = 87$ kHz. At this frequency, atoms are driven to the second band and lost by Landau–Zener tunneling, leading to a flat shoulder in the distribution

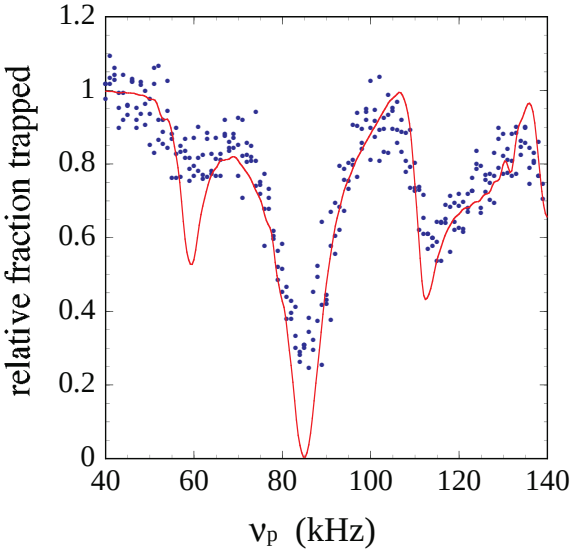

Fig. 6. Wannier–Stark ladder resonances. Each point represents an experimental run as shown in Fig. 5. The fraction of trapped atoms is normalized to the number that is trapped when no modulation is applied (Fig. 5a). For this spectrum, the experimental parameters are as follows: $V_0/h = 75 \pm 7$ kHz, $a = 1570 \pm 10$ m/s^2, $\lambda = 0.096 \pm 0.002$. The final velocity was 1.2 m/s. The solid line is a quantum numerical simulation, which uses the experimental parameters

used to normalize the distributions with the phase modulation on. In Fig. 5b, the modulation frequency was set at a Wannier–Stark resonance, and the accelerated peak is nearly gone. In this case, there is a flat shoulder corresponding to atoms that are driven out of the well during the acceleration. Because the final velocity is fixed, we change the linear ramp time of the frequency offset to obtain different accelerations. The ramp times were varied in the range from 650 μs to 1000 μs, corresponding to accelerations that range from 1200 m/s^2 to 1800 m/s^2. A spectrum is measured by scanning ν_p in 1 kHz steps over a range of (typically) 100 kHz, and each frequency step is repeated several times. The amplitude of phase modulation was adjusted to optimize the visibility of the resonances. We found that the optimum was $\lambda = 0.096$ where a 50% increase in the amplitude caused noticeable broadening. The laser intensity and detuning were adjusted to give $V_0/h = 68$ kHz; this value gave the desired band structure that is shown in Fig. 1.

An example of a measured spectrum is shown in Fig. 6; it has two clear resonances which are necessary to determine the Wannier–Stark splitting. The theoretical curve is the result of a numerical integration of the time-dependent Schrödinger equation that used the experimental conditions [9]. In our first measurements of the spectra, the resonances were resolved but broader than predicted by the numerical simulations. We found that this was due to the small Gaussian variation of the well depth for atoms that move transversely with respect to the standing wave. The absolute locations of the resonances are sensitive to the well depth, and as atoms move transversely across the spatial Gaussian profile of the standing wave their resonances shift. The resonant frequencies are in the range of 100 kHz, while the splittings are three to four times smaller: therefore even a 5% variation of the resonant frequency is significant. To verify this picture, we limited the binning window on the 2-D images so that in one transverse direction we restricted our measurement to a subset of colder atoms. We found that this procedure gave narrower resonances, and it was used in all the data that are shown.

The Wannier–Stark splitting as a function of acceleration was determined from a range of spectra, and the results are shown in Fig. 7. These results are consistent with the predicted linear scaling, within the experimental uncertainty. The range of possible accelerations was limited in the experiment to the range from 1200 m/s^2 to 1800 m/s^2: for smaller accelerations, the resonances are not cleanly resolved due to the variation in well depth over the atomic sample, while for larger accelerations the splitting becomes comparable to the width of the second band.

A simple physical picture of quantum interference from multiple temporal slits can be used to describe the Wannier–Stark ladder. The probability of absorption of a weak AC probe was derived for the case of a one-dimensional lattice in an external DC electric field [18]; however, the interpretation of the results as a quantum interference effect was not

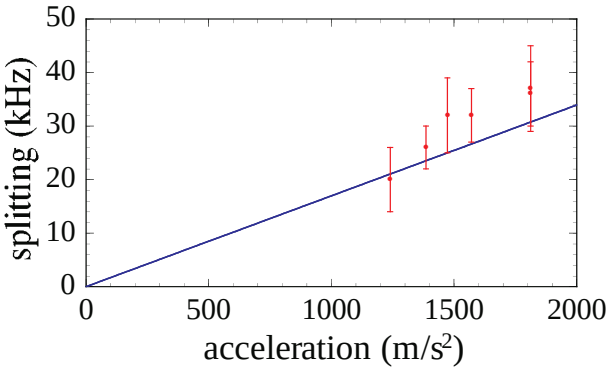

Fig. 7. Splitting between Wannier–Stark ladder resonances as a function of standing-wave acceleration. Each splitting was measured from a spectrum as shown in Fig. 6, for a range of different accelerations, and with the other parameters kept the same. The theoretical prediction of $\Delta\nu = aM/2\hbar k_L$ is given by the solid line

discussed. To explain this effect, consider an atom in the lowest energy band undergoing Bloch oscillations across the first Brillouin zone. The resonance condition for a weak phase modulation (frequency ν_p) occurs at $\pm k_0$, as shown in Fig. 2. During one Bloch period T_B, the atom experiences two resonant drives separated in time. The probability for an atom to make a transition to the second band after undergoing N Bloch oscillations was shown [18] to be proportional to

$$\frac{\sin^2(\beta_b N/2)}{\sin^2(\beta_b/2)}, \tag{3}$$

where β_b is a function of ν_p. This is the result for multiple-slit interference and is most familiar in the context of optics [19]. Temporal quantum interference provides physical insight for the appearance of the Wannier–Stark ladder, but it cannot predict the details of the spectrum (Fig. 6), such as the peak height, the width and the exact locations of the resonances.

2 Atomic tunneling

Tunneling of atoms through a barrier should become an important process at sufficiently low temperatures. A possible candidate for such an experiment would be an ultracold atom incident on a sheet of blue-detuned light that forms a one-dimensional repulsive optical dipole potential [14]. The barrier height could easily be controlled by adjusting the laser intensity. The difficulty with this experiment is that the barrier width is very large, because focusing of a sheet of light is limited to several micrometers, making the tunneling probability extremely small. The small focus also entails rapid divergence of the beam, leading to a spread in barrier width. The parameters required for such an experiment appear to be very difficult to attain.

The problem with the barrier width can be solved by using the accelerating standing wave. A simple picture of the atomic tunneling process can be obtained by transforming the potential into the co-moving coordinates of the accelerated atoms, $V_0 \cos(2k_L x') + Max'$, where M is the mass of the atom and x' is the coordinate in the accelerated frame. In the co-moving frame, the atoms see a "washboard potential" and escape via tunneling. The barrier width in this case can be much less than the wavelength of light, achieving the desired goal. Another advantage of this approach is that the signature for tunneling is in momentum space rather than real space. It is interesting to ask what is the largest acceleration that can be imposed on an atom for a given well depth?

There is clearly a classical limit to the tilt, when there are no local minima in the potential. This occurs for $a_{cl} = 2k_L V_0/M$, and for accelerations smaller than this value a particle can be stably trapped in one of the wells. Quantum mechanics, however, allows for tunneling from the wells to the continuum, in striking contrast to the classical prediction, and this effect can become important for accelerations that are much smaller than the classical limit.

A complimentary model of tunneling from the accelerating periodic lattice can be developed using the reciprocal lattice. Atoms are initially prepared in the lowest band. When the standing wave is accelerated, the wave number changes in time, and the atoms undergo Bloch oscillations across the first Brillouin zone. As the atoms approach the band-gap, they can make Landau–Zener transitions to the next band. Once the atoms are in the second band, they rapidly undergo transitions to the higher bands and are effectively free particles [9].

To observe tunneling in our experiment, we recognized that atoms initially trapped in the MOT can be (1) trapped and accelerated by the standing wave for the duration of the experiment, (2) trapped for some time before tunneling out of the wells, or (3) not trapped at all by the standing wave. The first category of atoms is the one of interest: the number of atoms in this group is proportional to the survival probability for the duration of the acceleration. To distinguish these surviving atoms from those that were lost from the wells, we implemented a three-step acceleration sequence using an arbitrary wave form generator to drive an acousto-optic modulator.

Figure 8 shows how the acceleration was varied to separate each category of atoms in velocity. After the MOT fields were turned off, the standing wave was turned on for 20 μs with zero acceleration; a portion of the cold atoms was trapped in the potential wells at this point. The potential was then accelerated at a (typical) rate $a_{slow} = 1500\,\mathrm{m/s^2}$ until the standing wave reached an intermediate velocity v_{int} (typically 1.05 m/s). This stage separated the trapped atoms from the rest of the distribution. The loss from the wells due to tunneling is negligible during a_{slow}. The acceleration was then switched to a higher value (a_{fast}) in the range 4500–10 000 $\mathrm{m/s^2}$, which changed the tilt of the potential, thus increasing the tunneling probability between the bound state and the continuum. After a controlled period of time T, the acceleration was switched back to a_{slow} in order to isolate the surviving atoms from those that had tunneled. This acceleration was maintained until the standing wave reached the final velocity v_f (typically 2.4 m/s), after which the beams were turned off. The acceleration sequence was measured in optical heterodyne on a digital storage oscilloscope. The time response of the standing wave to accelerations was determined by imposing phase modulation and measuring the modulation index as a function of the drive frequency. We found that the total switching time was less than 500 ns.

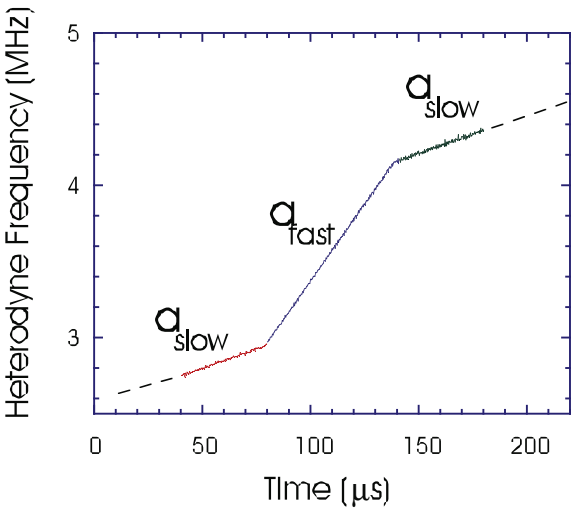

Fig. 8. The three-stage acceleration process used to study tunneling. This figure is a digitized heterodyne signal of the two counterpropagating beams, taken as the frequency difference was varied. A slope of 5.1 kHz/μs corresponds to an acceleration of 1500 $\mathrm{m/s^2}$

The two-peaked distribution shown in Fig. 9a represents atoms trapped and accelerated to v_f, for $a_{slow} = 1500\,m/s^2$ and $T = 0$. The large peak centered around $x = 0$ corresponds to atoms that were not trapped by the standing wave. The small peak at $x = 7$ mm corresponds to atoms that remained trapped and were accelerated to v_f; the area of this peak is proportional to the number of these atoms. The clean separation of the two peaks for a_{slow} indicates that tunneling is negligible, and this is supported by a theoretical analysis described below. The distribution in Fig. 9b is for the case in which $a_{fast} = 10\,000\,m/s^2$ and $T = 47\,\mu s$. It shows a three-peak distribution. The middle asymmetric peak represents atoms that tunneled out of the wells, and the peak on the right represents the surviving atoms. The normalization is taken to be the total area under these two peaks, which is proportional to the number of atoms initially prepared in the lowest band.

To determine a decay rate, we varied T and measured the survival probability with all the other parameters fixed. The result of a typical run is displayed in Fig. 10a, and it clearly demonstrates an exponential decay in the survival probability. The slope of this curve is a measurement of the tunneling rate Γ.

In order to claim that the loss of atoms is due to tunneling, it is necessary to rule out other loss mechanisms which would also appear as an exponential decay. Several possibilities are amplitude and phase noise of the optical potential, switching between different accelerations, beam pointing stability and spontaneous scattering. As we show below, these effects are negligible over the short (several hundreds of microseconds) duration of the experiment. These same effects, however, can pose very serious limitations on longer time scales, such as in experiments to observe Bloch tunneling in an optical lattice, or in optical dipole force traps for Bose condensation.

The amplitude and phase noise were studied using photodiode signals and optical homodyne measurements respectively. The signal levels of phase noise in these experiments were far below those required to cause any observable loss of atoms in our study of Wannier–Stark ladders [10]. Depletion of the trapped atoms could be induced by adding a much larger level of phase noise. The amplitude of each run was monitored on a digital storage oscilloscope, and traces with

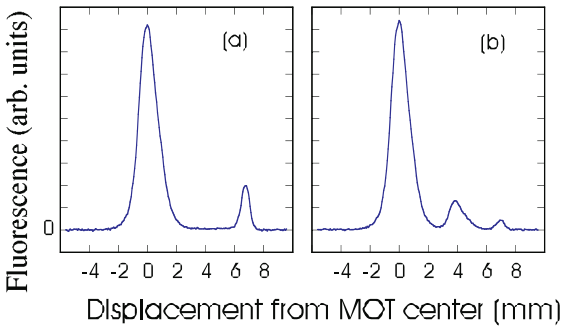

Fig. 9a,b. The distribution of atoms after exposure to an accelerating standing wave. The displacement is the distance from the atoms' initial location in the magneto-optic trap. The fluorescence is proportional to the number of atoms at a given displacement. In **a** a fraction of the atoms was trapped by the standing wave and accelerated for 1500 μs to a final velocity of 2.2 m/s. The atoms then drifted ballistically for 3 ms, allowing them to separate spatially from the main distribution. Here $V_0/h = 92$ kHz. In **b** a fast acceleration of $10\,000\,m/s^2$ was turned on for a duration of 47 μs, leading to substantial tunneling

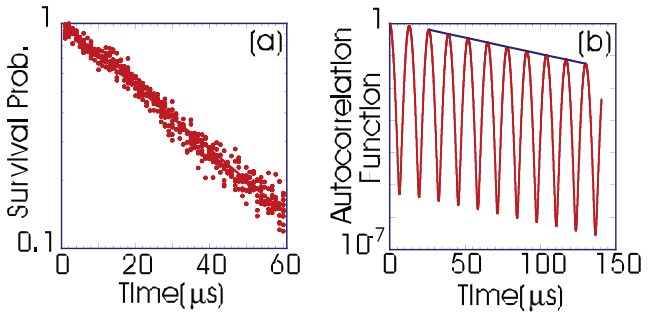

Fig. 10. a An example of an experimentally measured survival probability for $a_{slow} = 1200\,m/s^2$, $a_{fast} = 4500\,m/s^2$ and $V_0/h = 50.8$ kHz as a function of the duration of the fast acceleration. Note that the vertical axes are logarithmic. The solid line is an exponential fit to the data. **b** The theoretical autocorrelation function (a projection of the time-evolved state on to the initial state) for the case $a = 4500\,m/s^2$ and $V_0/h = 55$ kHz. The solid line is an exponential fit to the peaks of the oscillations, starting from the third peak to avoid short-time, non-exponential effects

amplitude spikes were rejected. Fast switching between different accelerations has high frequency components which could possibly drive atoms out of the wells. We checked this by varying the switching times, but did not observe any such loss. Spontaneous scattering could induce loss from the accelerating potential and must be minimized in order to study tunneling. For the experiments described here, the probability of spontaneous scattering is estimated to be 10% for an interaction time of 1 ms. Since the period of large acceleration was at most 200 μs, the spontaneous scattering probability during that crucial interval is negligible. In general, we did not observe any loss of atoms during a_{slow} which would have appeared as a shoulder between the two peaks.

We now show that the observed decay rates are in good agreement with the predictions of quantum mechanics. Figure 11 displays our measurements of $(\Gamma)^{-1}$ as a function of acceleration. The well depth in this case was $V_0/h = 72$ kHz, with an uncertainty of ±10%. The corresponding band structure in the absence of acceleration has one band contained within the wells with a width of 5 kHz. The gap between the first and second bands is 70 kHz, and the second band has a width of 40 kHz. The dashed curve is a theoretical prediction of the tunneling rate from Landau–Zener (L–Z) theory, $\Gamma_{LZ} = (a/2v_r)\exp(-a_c/a)$. Here $a_c = 2\pi(E_{gap}/2)^2/2\hbar^2 k_L$ is a critical acceleration, where E_{gap} is the energy gap between the first and second bands [2, 9]. This formula is derived from a simple two-level model with an avoided crossing between the levels, assuming that the transition only occurs at the avoided crossing. It is frequently used in atomic and molecular physics to describe collisions: however, it is difficult in those cases to obtain the L–Z rates from first principles, due to the complexity of the potential curves. The present atom optics system provides a unique opportunity for absolute comparison with theory, and it is interesting to see how the tunneling rate compares with the L–Z prediction. We see that the experimental points (solid dots) approximately follow the L–Z prediction, but clearly display oscillations as a function of the acceleration. At large values of the acceleration, the results approach the L–Z curve, while at the smaller values the deviations become larger and sharper.

What is the physics behind these oscillations? The L–Z model assumes that the inter-band transitions occur only at the band gaps (the points of closest approach between the

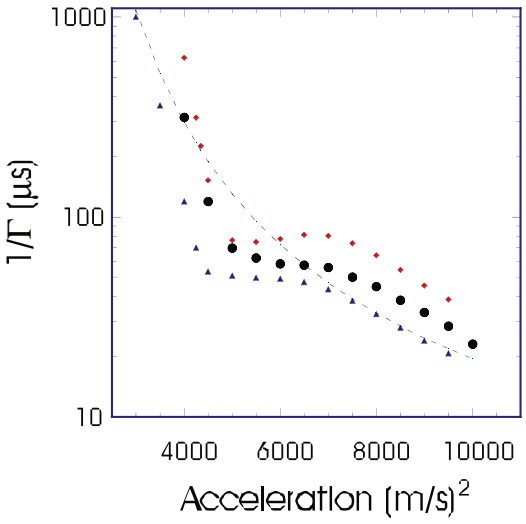

Fig. 11. The tunneling lifetime as a function of acceleration. The experimental data are marked by solid dots. The uncertainty in the exponential fits which determine Γ is typically $\pm 2\%$, and the uncertainty in the acceleration for the range shown is $\pm 50\,\mathrm{m/s^2}$. The dashed line is the prediction of L–Z theory. The experimental well depth was $V_0/h = 72$ kHz, with an uncertainty of $\pm 10\%$. The data are bracketed between quantum simulations for wells depths of $V_0/h = 60$ kHz (solid triangles) and $V_0/h = 72$ kHz (solid diamonds), and the L–Z prediction is for an intermediate value, $V_0/h = 66$ kHz

bands), and that there are no correlations between successive periods of the Bloch oscillation. In the present system, the band curvature is not large, and transitions are no longer limited to the gap but can occur at different points along the band. A theoretical analysis of this problem shows that, in a single Bloch period, there are contributions to the tunneling probability at points of both nearest and farthest approach between the bands, where their slope is zero [20, 21]. Contributions from other points along the band cancel out. This leads to interference effects in the tunneling probability, which depend on the Bloch period. The period of oscillation in the tunneling rate (as a function of acceleration) is proportional to a, while the amplitude of the oscillation is inversely proportional to a. At smaller values of the acceleration, deviations about the L–Z prediction are considerably larger. This is physically reasonable, because coherent effects become dominant when tunneling out of the second band is slow compared to the Bloch period. The extreme case is the coherent regime of Bloch oscillations and Wannier–Stark ladders, where tunneling from the trapped state plays no role. The interplay between coherent and irreversible effects has been studied theoretically and observed, for example, in atomic physics experiments [22, 23]. The present experiments, however, enable a detailed study of these effects in a much simpler setting, and with no adjustable parameters.

These oscillations are also seen in the quantum simulations shown in Fig. 11, where the time-dependent Schrödinger equation is solved for $a = a_{\mathrm{fast}}$. The initial condition is simply taken to be the lowest state of the potential with $a = 0$ and its survival probability is the projection of the time-dependent solution on to the initial state. As seen from Fig. 10b, this autocorrelation function exhibits Bloch oscillations with decaying amplitude. The decay of the peaks is clearly exponential, and the computed time constant for this ideal calculation provides the tunneling rate used in the comparison with experiment. The largest experimental uncertainty for this comparison with theory is in the well depth V_0 ($\pm 10\%$), and the experimental data are bracketed between two numerical simulations. Given the high sensitivity of tunneling rate to the well depth, the agreement with *an ideal simulation* over the range of accelerations is quite good, and further confirms the observation of tunneling.

3 Summary

In summary, our observations of Wannier–Stark ladder resonances and tunneling of ultracold atoms, combined with the recent results of the ENS group, establish atom optics as an new testing ground for quantum transport. We have recently extended this work to observe short-time deviation from exponential decay, a basic quantum effect that was predicted over 40 years ago, but not seen experimentally until now [24–26]. In future studies of the Wannier–Stark ladder, we will work to reduce the variation in well depth over the atomic sample. This should enable the measurement of the spectrum for smaller values of the acceleration, and should allow a detailed study of the complex line shapes. Improved signal-to-noise should also enable a measurement of tunneling rates at smaller accelerations, where the deviations from L–Z theory are most important. The study of non-exponential decay will focus on the question of inhibition of tunneling by repeated measurement, and should address issues of irreversibility and measurement in a simple and controlled quantum system.

Acknowledgements. We are grateful to C. Salomon and E. Mendez for stimulating discussions. The work of M.G. Raizen was supported by the US Office of Naval Research, the R.A. Welch Foundation and the US National Science Foundation. The work of Qian Niu was supported by the R.A. Welch Foundation. Bala Sundaram is grateful for the support of the US National Science Foundation.

References

1. F. Bloch: Z. Phys. **52**, 555 (1929)
2. C. Zener: Proc. R. Soc. London A **145**, 523 (1934)
3. N.W. Ashcroft, N.D. Mermin: *Solid State Physics* (Saunders College, 1976)
4. G.H. Wannier: Phys. Rev. **117**, 432 (1960)
5. J. Zak: Phys. Rev. **20**, 1477 (1968); A. Rabinovitch: Phys. Lett. **33A**, 403 (1970)
6. Y. Gefen, E. Ben-Jacob, A.O. Caldeira: Phys. Rev. B **36**, 2770 (1987)
7. E.E. Mendez, G. Bastard: Phys. Today 34 (1993)
8. M.G. Raizen, C. Salomon, Q. Niu: Phys. Today 30 (1997)
9. Qian Niu, Xian-Geng Zhao, G.A. Georgakis, M.G. Raizen: Phys. Rev. Lett. **76**, 4504 (1996)
10. S.R. Wilkinson, C.F. Bharucha, K.W. Madison, Qian Niu, M.G. Raizen: Phys. Rev. Lett. **76**, 4512 (1996)
11. C.F. Bharucha, K.W. Madison, P.R. Morrow, S.R. Wilkinson, Bala Sundaram, M.G. Raizen: Phys. Rev. A **55**, R857 (1997)
12. M. Ben Dahan, E. Peik, J. Reichel, Y. Castin, C. Salomon: Phys. Rev. Lett. **76**, 4508 (1996)
13. E. Peik, M. Ben-Dahan, I. Bouchoule, Y. Castin, C. Salomon: Phys. Rev. A **55**, 2989 (1997)
14. A.P. Kazantsev, G.I. Surdutovich, V.P. Yakovlev: *Mechanical Action of Light on Atoms* (World Scientific, Singapore 1990) pp. 58–60
15. C. Cohen-Tannoudji: In *Fundamental Systems in Quantum Optics*, Les Houches, 1990, ed. by J. Dalibard, J.M. Raimond, J. Zinn-Justin (Elsevier 1992)
16. S. Chu: Science **253**, 861 (1991)
17. F.L. Moore, J.C. Robinson, C. Bharucha, P.E. Williams, M.G. Raizen: Phys. Rev. Lett., **73**, 2974 (1994)

18. J.B. Krieger, G.J. Iafrate: Phys. Rev. B **33**, 5494 (1986); Q. Niu: Phys. Rev. B **40**, 3625 (1989); M.C. Chang, Q. Niu: Phys. Rev. B **48**, 2215 (1993)
19. E. Hecht: *Optics* (Addison Wesley, Reading, MA 1989)
20. P. Ao, J. Rammer: Phys. Rev. Lett. **62**, 3004 (1989)
21. S. Dyrting, B. Sundaram: in preparation
22. J.E. Avron: Phys. Rev. Lett. **37**, 1568 (1976); Ann. Phys. (N.Y.) **143**, 33 (1982)
23. L. Sirko, S. Yoakum, A. Haffmans, P.M. Koch: Phys. Rev. A **47**, R782 (1993)
24. P.T. Greenland: Nature **335**, 298 (1988)
25. P.T. Greenland: Nature **387**, 548 (1997)
26. S.R. Wilkinson, C.F. Bharucha, M.C. Fischer, K.W. Madison, P.R. Morrow, Q. Niu, B. Sundaram, M.G. Raizen: Nature **387**, 575 (1997)